Electronic structure and magnetic symmetry in MnTiO_{3} analyzed by second harmonic generation

Judy G. Cherian, Takahisa D. Tokumoto, Haidong Zhou, Eun Sang Choi, and Stephen A. McGill

Electronic structure and magnetic symmetry in MnTiO$_3$ analyzed by second harmonic generation

Judy G. Cherian,[1,2] Takahisa D. Tokumoto,[1] Haidong Zhou,[1,*] Eun Sang Choi,[1] and Stephen A. McGill[1,†]

[1] *National High Magnetic Field Laboratory, 1800 E. Paul Dirac Dr., Tallahassee, FL 32310*
[2] *Department of Physics, Florida State University, Tallahassee, FL 32306*
(Dated: May 22, 2013)

Second harmonic generation (SHG) and linear absorbance spectra of MnTiO$_3$ were measured and the 1.88, 2.41, 2.63, and 3.06 eV SHG features were identified as *d-d* optical transitions from $^6A_{1g}$ to $^4T_{1g}(^4G)$, $^4T_{2g}(^4G)$, $\{^4E_g,^4A_{1g}(^4G)\}$, and $^4E_g(^4D)$ respectively. These zero-phonon transitions were used to calculate the octahedral crystal field splitting energy (Δ_0) and the Racah parameters B and C. The SHG spectra showed significant distinctions between the antiferromagnetic and the paramagnetic or spin-flop phases. The polarization dependence of the SHG in the spin-flop phase provided optical evidence that the spins canted from the *c*-axis toward the *a*-axis. These distinctions between the three magnetic phases could be useful for mapping 180° antiferromagnetic domains in MnTiO$_3$.

I. INTRODUCTION

Titanate materials, with chemical formula $RTiO_3$ (R = Ca, Sr, Ba, Mn), have captured interest for both fundamental and applied study[1–3]. These materials usually exhibit one or more ferroic orders. Therefore, they are highly beneficial in understanding the physics behind the coupling of these coexisting orders, such as in magneto-electric coupling. It has also been reported that these materials are important for technological applications such as memory devices and solar cells[3–11]. Antiferromagnetic $MnTiO_3$ (T_N = 64 K), exhibiting ilmenite structure, possesses a magnetic field induced spin-flop phase (H_c = 6.5 T), and it further exhibits a linear magnetoelectric (ME) effect[12–14]. It is thought that the spin-flop phase might also display ferrotoroidic order[12], which is a novel state characterized by a spontaneously ordered vortex of spins. Ferrotoroidic order is considered potentially to be a fourth type of ferroic order[15,16]. Here, we undertake an optical analysis of the electronic and magnetic structure of $MnTiO_3$ using linear absorption spectroscopy and second harmonic generation.

Second harmonic generation (SHG) is a convenient and effective tool for probing the symmetry of electronic and magnetic states[17–20]. The enhancement of SHG near an optical resonance makes it a sensitive probe of electronic energy levels including d-d transitions[21–23]. Since SHG spectra are affected by symmetry changes, the spectra should be distinct for the paramagnetic, antiferromagnetic, and spin-flop phases. Therefore, one can use SHG for understanding both the structure and symmetry of the crystallographic and magnetic orders in $MnTiO_3$. In linear absorption techniques, magnetic symmetry can be determined by analyzing the relationship between the magnetic order and collective excitations like excitons and magnon sidebands[24]. In light of the interesting properties and behavior exhibited by $MnTiO_3$, we used SHG to probe its electronic structure. We also analyzed the spectral and temperature dependence of the lowest-order non-linear optical susceptibilities in $MnTiO_3$ using polarization-dependent SHG.
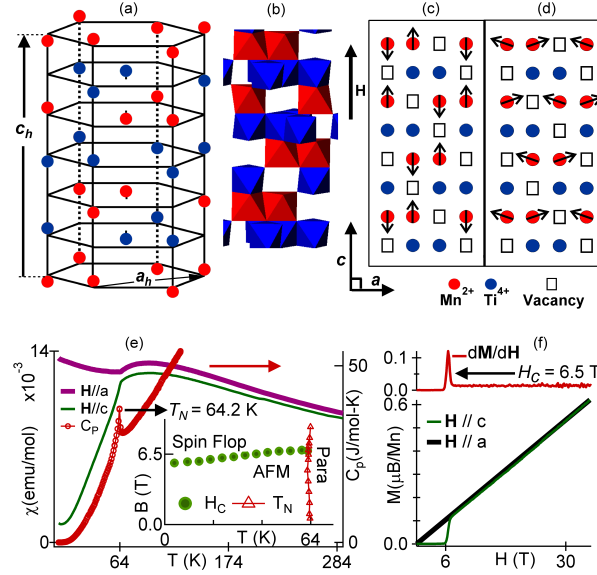

FIG. 1. Schematic illustrations of (a) cation sublattice and (b) MnO_6 and TiO_6 octahedra of $MnTiO_3$. (c) The collinear spin structure along the c-axis with $H\|c$ and $H < H_c$. (d) A proposed non-collinear spin structure with spins canting to a-axis with $H\|c$ and $H > H_c$. (e) Temperature dependence of magnetic susceptibility and specific heat. The inset shows the phase diagram of $MnTiO_3$ (adapted from Fukata *et al.*[29]). (f) Magnetic field dependence of magnetization and the derivative of magnetization along the c-axis at $T = 1.4$ K.

II. STRUCTURE AND PROPERTIES OF $MnTiO_3$

In titanates possessing ilmenite structure (R= Fe, Mn, Zn), the oxygen atoms form a close-packed hexagonal structure with Mn^{2+} and Ti^{4+} ions in alternate planes, occupying two-thirds of the available octahedral interstitial sites (Figs. 1(a,b)). The electrostatic repulsion between Mn^{2+} and Ti^{4+} leads to them being alternately displaced above and below the hexagonal layers in the ab-plane[25,26]. The Mn-O octahedra undergo a slight trigonal distortion, and the Mn^{2+} cations are in the high spin $3d^5$ state as confirmed by electron energy loss spectroscopy (EELS)[25–28].

$MnTiO_3$ single crystals were synthesized by the floating zone method in an image furnace. These crystals were oriented by Laue diffraction, cut along the ab-plane, and polished to optical quality. They were paramagnetic at room

temperature (Fig. 1(e) inset) and belong to the non-magnetic, centrosymmetric point group $\overline{3}$[25,27,29–31]. Magnetic susceptibility (Fig. 1(e)) measurements confirmed that, around 64 K, the Mn^{2+} magnetic moments oriented along the c-axis (AFM phase). In $MnTiO_3$, the Mn^{2+} spins align antiferromagnetically along the c-axis and also within the ab-plane as depicted in Fig. 1(c).

The spin-flop transition in $MnTiO_3$ (H_c= 6.5 T) was observed by the jump in c-axis magnetization to match the a-axis trend (Fig. 1(f)) at 6.5 T, which additionally demonstrated the canting of spins from the c-axis into the a-axis[13]. One possible spin arrangement in this phase is shown in Fig. 1(d). $MnTiO_3$ has a spin structure similar to that of Cr_2O_3, which is another material with a linear ME effect[12,32,33]. In the spin-flop phase of Cr_2O_3, its ME tensor acquires non-zero antisymmetric off-diagonal terms, and this is indicative of non-zero toroidic moments above the critical spin-flop magnetic field[34]. The linear magnetoelectric effect in $MnTiO_3$ has been experimentally verified by Mufti *et al*[14]. Therefore, $MnTiO_3$ has also been proposed as a possible ferrotoroidic candidate.

III. NON-LINEAR OPTICAL SUSCEPTIBILITIES AND THEIR RELATION TO SHG SPECTRAL INTENSITY

Second harmonic generation spectroscopy is recognized as a sensitive experimental technique for probing the symmetry of antiferromagnets[17–20]. The main physical processes that contribute to SHG are the electric dipole (ED) transitions, which are proportional to the induced electrical polarization, magnetic dipole (MD) transitions ($\propto$ induced magnetization), and electric quadrupole (EQ) transitions ($\propto$ quadrupole polarization).

In $MnTiO_3$, above the Néel temperature (T_N= 64 K), the centro-symmetric point group $\overline{3}$ permits only i-type (time-symmetric) axial tensors of rank three while any time-antisymmetric (c-type) tensors are forbidden; thus only MD transitions contribute. However, below T_N, the point group becomes $\underline{\overline{3}}$[14,30,31,35], due to the antiferromagnetic ordering of spins breaking both spatial and temporal symmetry. However, the combined space-time-reversal operation, $\underline{\overline{1}}$, remains a symmetry element.[36] Consequently, c-type polar tensors are also allowed resulting in an induced polarization; accordingly, both ED and MD transitions are allowed for the AFM phase. Specific heat measurements (Fig. 1(e)) provided evidence for a continuous phase transition around 64 K, and prior magnetocapacitance measurements revealed no dielectric anomaly in zero magnetic field at T_N (also confirmed in our samples)[14]. Therefore, no change in lattice symmetry was observed at T_N and so the MD process was related to the crystalline structure, while the ED process was related to the magnetic structure[31]. Even though electric quadrupole contributions are allowed above and below the Néel temperature, the SHG signal we observed could be unambiguously interpreted by restricting the analysis to the MD and ED processes. The inclusion of electric quadrupole contributions added more terms to the SHG intensity without revealing any behavior that was qualitatively different from that already produced by MD and ED processes. A more detailed calculation of the SHG intensity which includes electric quadrupole terms is provided in the Supplementary Information.

The fundamental equations describing SHG produced by ED and MD transitions in $MnTiO_3$ are $\mathbf{P}(2\omega) \propto \chi_{ijk}\mathbf{E}(\omega)\mathbf{E}(\omega)$ and $\mathbf{M}(2\omega) \propto \chi_{ijk}\mathbf{E}(\omega)\mathbf{E}(\omega)$, respectively. The third rank, non-linear optical susceptibility tensor, χ_{ijk}, will be axial for magnetization and polar for electrical polarization. Even though symmetry allowed, processes like $\mathbf{P}(2\omega) \propto \chi_{ijk}\mathbf{E}(\omega)\mathbf{H}(\omega)$ are not included since d-d transitions in $MnTiO_3$ are parity forbidden. Based on these observations, the seven independent components of the non-linear susceptibility tensor for this point group can be deduced[36]. However, by aligning the sample in such a way that the light propagation direction (z-axis) is along the crystallographic c-axis, only three of the components are to be considered for SHG analysis. They are as follows[36]: $\chi^{(1)} = \chi_{xxx} = -\chi_{yyx} = -\chi_{yxy} = -\chi_{xyy}$, $\chi^{(2)} = \chi_{yyy} = -\chi_{xxy} = -\chi_{xyx} = -\chi_{yxx}$, and $\chi^{(3)} = \chi_{zxx} = \chi_{zyy}$.

We can use Maxwell's equations to derive the wave equation for SHG in a material with the given point group symmetry. The contribution of i-type susceptibility (above and below T_N) towards non-linear magnetization is given by[20,37,38]

$$\mathbf{M}_{NL} = \epsilon_0 \frac{c}{n} \begin{pmatrix} \chi_{i1}(E_x^2 - E_y^2) - 2\chi_{i2}E_xE_y \\ -2\chi_{i1}E_xE_y - \chi_{i2}(E_x^2 - E_y^2) \\ \chi_{i3}(E_x^2 + E_y^2) \end{pmatrix} . \tag{1}$$

On the other hand, below T_N, non-linear polarization due to the c-type tensor will be given by an expression similar to that of induced magnetization with the i-type tensor replaced by the c-type tensor[37,38]. Thus, the induced non-linear polarization and magnetization act as source terms for the wave equation of electric field[20,37,38]. We can express the

total source term in a circularly polarized basis as,

$$\vec{S} = 4\sqrt{2}\frac{\omega^2}{c^2}\bigg(\left[(-\chi_{i2}+\mathrm{i}\chi_{i1}) + (\chi_{c1}+\mathrm{i}\chi_{c2})\right]E_-^2\,\hat{\mathbf{e}}_+$$
$$+ \left[(\chi_{i2}+\mathrm{i}\chi_{i1}) + (-\chi_{c1}+\mathrm{i}\chi_{c2})\right]E_+^2\,\hat{\mathbf{e}}_-$$
$$+ \sqrt{2}\chi_{c3}E_+E_-\,\hat{\mathbf{e}}_z\bigg) \tag{2}$$

where $E_\pm$ refer to the two components of circular polarization, $\hat{\mathbf{e}}_\pm$ represents the unit vectors of circular polarization, and $\hat{\mathbf{e}}_z$ is the unit vector along z-axis. From this expression it is evident that the helicity of the SHG signal will be opposite to that of the incident circular polarization. The total intensity of the SHG signal can be calculated as follows:

$$I \propto \left[|\chi_{i1}|^2 + |\chi_{i2}|^2 + |\chi_{c1}|^2 + |\chi_{c2}|^2\right](E_+^4 + E_-^4)$$
$$-2\left[\chi_{i2}^{'}\chi_{c1}^{'} + \chi_{i2}^{''}\chi_{c1}^{''}\right](E_+^4 + E_-^4)$$
$$+2\left[\chi_{i1}^{'}\chi_{c2}^{'} + \chi_{i1}^{''}\chi_{c2}^{''}\right](E_+^4 + E_-^4)$$
$$+2\left[\chi_{c2}^{''}\chi_{c1}^{'} - \chi_{c2}^{'}\chi_{c1}^{''}\right](E_+^4 - E_-^4)$$
$$+2\left[\chi_{i2}^{''}\chi_{i1}^{'} - \chi_{i2}^{'}\chi_{i1}^{''}\right](E_+^4 - E_-^4)$$
$$+2\left[\chi_{i2}^{''}\chi_{c2}^{'} - \chi_{i2}^{'}\chi_{c2}^{''}\right](E_+^4 - E_-^4)$$
$$+2\left[\chi_{i1}^{''}\chi_{c1}^{'} - \chi_{i1}^{'}\chi_{c1}^{''}\right](E_+^4 - E_-^4), \tag{3}$$

where the single and double primes refer to the real and imaginary parts, respectively.

The first three terms in the above expression for SHG intensity contain the sum of left and right incident intensities $(E_+^4 + E_-^4)$; hence, their combined value (for the given tensor components) is independent of the polarization of the incoming beam. However, the last four terms involve the difference between the intensities $(E_+^4 - E_-^4)$; therefore, they can be defined as "polarization dependent terms". The combined value of these polarization dependent terms (for the given tensor components) will change sign with the helicity of circular polarization, while it is zero for linear polarization. Therefore, these terms account for a circular polarization dependence in the SHG intensity. According to Fiebig *et al.*, the change in the incident circular polarization is equivalent to a time reversal or change in the antiferromagnetic domain vector[20]. In other words, the change in the SHG intensity can be brought about by either changing the incident circular polarization or by moving the laser spot on the sample so as to orient the incident light on a different domain in which the antiferromagnetic vector is reversed. This mixing of the MD (crystalline) and ED (magnetic) contributions in the polarization dependent terms forms the basis of imaging 180° domains via SHG[20].

We used a Coherent Legend regeneratively amplified laser (800 nm, 1 kHz rep rate, 150 fs) coupled with a TOPAS optical parametric amplifier (OPA), to generate light in the range of 670 nm to 1400 nm. The incident light was focused on the sample placed in an Oxford Spectromag (1.6 K, 10 T). SHG was collected in transmission geometry and optical filters were used to remove the incident fundamental from the transmitted SHG. The signal was amplified using a photomultiplier tube (PMT) coupled to a monochromator. The photocurrent from the PMT was collected by a boxcar integrator and read by a digital multimeter. Quarter waveplates and glan polarizers were used in the incident and transmitted beams to select the desired circular polarization in each path.

IV. RESULTS AND DISCUSSION

A. Optical transitions and electronic structure of MnTiO$_3$ using SHG

Figure 2 shows the room temperature second harmonic spectrum of MnTiO$_3$ measured using linearly polarized excitation. The room temperature and 4 K absorbance spectra with the partial Tanabe-Sugano energy level diagram of Mn^{2+} ions in high-spin $3d^5$ configuration are also shown. Under the influence of crystal field, the Mn^{2+} d-orbitals undergo splitting with a crystal field stabilization energy (CFSE) of zero[39]. The influence of a trigonal distortion on crystal field is disregarded since the high-spin state of Mn^{2+} cations denies further enhancement of CFSE[28,39].
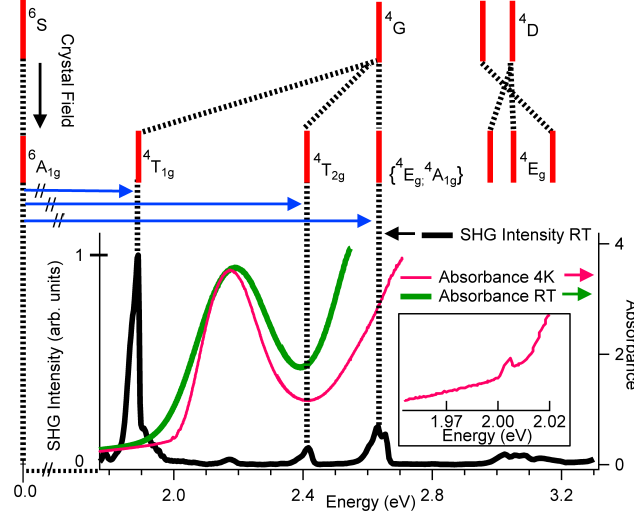
FIG. 2. The room temperature SHG spectrum of MnTiO$_3$ (black line) in the 1.77 eV to 3.74 eV range with linearly polarized light ($\mathbf{k} \parallel c$-axis). The SHG peaks represent the various optical transitions from the ground state of high-spin Mn^{2+} cations in a trigonally distorted octahedral crystal field ($^6A_{1g}$) to the excited states as shown in the high-spin $3d^5$ Tanabe-Sugano energy level diagram. The small SHG peak at 2.19 eV is a background artifact. Absorbance spectra using unpolarized light ($\mathbf{k} \parallel c$-axis) at room temperature and 4 K show the $^6A_{1g}$ to $^4T_{1g}$ peak at a higher energy compared to the corresponding SHG peak. Inset shows a collective excitation at 2 eV in the 4 K absorbance spectrum.

All d-d transitions in MnTiO$_3$ are electric-dipole forbidden per Laporte and spin selection rules. However, the linear absorption spectrum showed strong absorption peaks which might indicate a substantial vibronic coupling that can make these transitions parity-allowed[24]. ED forbidden transitions which become allowed due to vibronic coupling are typically blue-shifted and broad compared to the zero-phonon lines (ZPL)[40]. We assign the linear absorption peak at 2.2 eV to the $^6A_{1g}$ to $^4T_{1g}(^4G)$ transition. The sharp increase in absorbance around 2.5 eV is ascribed to higher d-d transitions and the onset of the charge transfer absorption edge. Evidence for vibronic coupling in linear absorption can be gleaned from the temperature dependence of the 2.2 eV peak, which narrows and red-shifts at 4 K. The fine structure at 2 eV in the 4 K absorbance spectrum (Fig. 2 inset) appears to be a collective excitation. These excitations, occurring near the band-edge, have been studied in similar materials[24,41,42].

The SHG spectrum obtained displayed significant differences from the linear absorption spectrum. The second harmonic signal can be enhanced when the fundamental or second harmonic frequency matches with an electronic transition[22]. Therefore, these narrow peaks, occurring at lower energies compared to the center positions of the linear absorption features, should correspond to optical transitions in MnTiO$_3$. The phonon contribution to the nonlinear magnetization or polarization is negligible since it is proportional to the second-order hyper-Raman tensor element $\left(\partial\chi^2(2\omega)/\partial q\right)$ where ∂q is the displacement of the atoms from their equilibrium position[43]. Consequently, we identify these room-temperature, MD allowed, SHG peaks as zero-phonon lines. We assign the 1.88, 2.41, and 2.63 eV SHG peaks in MnTiO$_3$ as the optical transitions from $^6A_{1g}$ to $^4T_{1g}(^4G)$, $^4T_{2g}(^4G)$, and $\{^4E_g,^4A_{1g}(^4G)\}$ respectively.

The SHG spectrum of MnTiO$_3$ can be further discussed in comparison to the linear absorption spectrum of MnPS$_3$, which also possesses high-spin Mn^{2+} cations[44] and trigonally distorted Mn-S octahedra, with the trigonal axis perpendicular to the ab-plane[45]. MnPS$_3$ undergoes antiferromagnetic ordering below 78 K and showed a spin-flop phase at high magnetic fields[45]. Grasso et $al.$ have identified the 1.92, 2.40, and 2.64 eV absorption peaks in MnPS$_3$ as the optical transitions from $^6A_{1g}$ ground state to the spin-forbidden $^4T_{1g}(^4G)$, $^4T_{2g}(^4G)$, and the degenerate $\{^4E_g,^4A_{1g}\}$ states respectively[46]. Room temperature fluorescence excitation spectra of MnPS$_3$ reported by Grasso et $al.$, revealed that the $^6A_{1g} \rightarrow {}^4E_g(^4D)$ transition will be exhibited at 3.13 eV[47]. The phosphorescence excitation spectrum of MnPS$_3$ at 4.2 K reported by Goates et $al.$, demonstrated this transition at 3.11 eV[48]. These results prompted us to think that the 3.06 eV SHG peak in MnTiO$_3$ may also correspond to the optical transition from the ground state to the $^4E_g(^4D)$ excited state.

We used these assignments to evaluate the octahedral crystal field splitting energy, Δ_0 ($10Dq$). The energy of the excited states relative to the ground state can be expressed in terms of $10Dq$ and the Racah B and C parameters as[39,46],

$$E\left[^4T_{1g}\right] = -10Dq + 10B + 6C - 26B^2/10Dq \rightarrow 1.88 \text{ eV},$$
$$E\left[^4T_{2g}\right] = -10Dq + 18B + 6C - 38B^2/10Dq \rightarrow 2.41 \text{ eV},$$
$$E\left[\{^4E_g,^4A_{1g}(^4G)\}\right] = 10B + 5C \rightarrow 2.63 \text{ eV},$$

$E\left[^4E_g(^4D)\right] = 17B + 5C \rightarrow 3.06$ eV.

From these expressions, we computed B=490 cm^{-1} (61 meV) and C=3200 cm^{-1} (400 meV). The average value of crystal field splitting energy $(10Dq)$ was found to be 8200 cm^{-1} (1.0 eV). Thus, from our comparison of linear absorbance and SHG spectra, it is evident that both measurements are beneficial in identifying the optical transitions when significant phonon coupling is likely present. However, the comparison also reveals that the SHG technique is better suited to resolve the various spectral transitions whereas linear techniques fail to do so. The observed SHG lines pointed toward significant vibronic coupling in MnTiO$_3$. Therefore, SHG can be a sensitive tool for understanding the electronic structure.

B. Tracking magnetic ordering with SHG

SHG spectra of MnTiO$_3$ were collected using a circularly polarized fundamental at 920 nm in the paramagnetic (80 K & 0 T), the antiferromagnetic (1.6 K & 0 T), and the spin-flop phases (1.6 K & 8 T). Fig. 3(a) shows the spectra in the paramagnetic state for left and right circularly polarized excitation. The non-zero SHG signal was due to the MD transitions allowed by the axial i-type tensors. The difference between the intensities of the left and right polarized SHG can be explained using the expression for total intensity (Eq. 3). Above T_N, the c-tensors are identically zero for centrosymmetric, non-magnetic crystals. Therefore, the expression for total intensity will be reduced to,

$$I_{para} = \left[|\chi_{i1}|^2 + |\chi_{i2}|^2\right](E_+^4 + E_-^4)$$
$$+2\left[\chi_{i2}^{''}\chi_{i1}^{'} - \chi_{i2}^{'}\chi_{i1}^{''}\right](E_+^4 - E_-^4). \tag{4}$$

For the individual components of circular polarization, one can rewrite Eq. 4 as,

$$I_{para} = \Bigg[\left(|\chi_{i1}|^2 + |\chi_{i2}|^2\right)$$
$$\pm 2\left(\chi_{i2}^{''}\chi_{i1}^{'} - \chi_{i2}^{'}\chi_{i1}^{''}\right)\Bigg]E_{\pm}^4. \tag{5}$$

In the above expression, it is clear that there is a polarization dependent term involving the components of the i-tensors. Therefore, due to mixing of the real and imaginary parts of the two i-type susceptibilities, the non-zero polarization dependent term in the paramagnetic phase created a circular intensity difference (CID) in the SHG intensity as exhibited in Fig. 3(a). The percent change between left and right polarization in the paramagnetic phase is shown in Fig. 3(d). The nature of CID in the resonance region requires special attention. It should be noted that the CID was negligibly small near the central wavelength of the resonance compared to elsewhere. Comparing Eq. 3 and Fig. 3(d), one can infer that it was the polarization dependent intensity term that went to zero at this point. As expected from the expression for the source terms (Eq. 2), the helicity of the SHG was observed to be opposite to that of the fundamental. On a comparative note, in the paramagnetic phase of Cr$_2$O$_3$, the polarization dependent intensity term was zero and its SHG spectrum showed no polarization dependence[20]. MnTiO$_3$ has a lower crystallographic symmetry than Cr$_2$O$_3$, and this lower symmetry caused the non-zero CID we observed in the paramagnetic phase of MnTiO$_3$.

The SHG spectra of MnTiO$_3$ in the zero-field AFM phase (Fig. 3(b)) displayed a pronounced CID which was significantly larger than the CID in the paramagnetic phase. Since the AFM phase is non-centrosymmetric, c-tensors are non-zero and hence, ED processes also contribute. Therefore, the SHG intensity is given by Eq. 3 rather than Eq. 4. It was evident that there were more polarization dependent terms in the AFM phase compared to the paramagnetic phase. Therefore, one can conclude that these extra polarization dependent terms created by the mixing of ED and MD processes were the source of the significantly increased CID in the AFM phase. In addition, the CID remained the same throughout the resonance and did not go to zero as in the paramagnetic state.

Comparing the SHG spectra in the AFM and paramagnetic phases, one can see that both exhibited a non-zero difference in the intensity of left and right polarized SHG. In the paramagnetic phase, the CID was very small near the central wavelength of the resonance. On the other hand, in the AFM phase, the CID was at least doubled compared to the paramagnetic phase, and it remained constant in the whole spectral region under consideration. In Fig. 3(e), we measured the temperature dependence of SHG CID from 3 K to 80 K. This plot shows that the transition in the SHG response between the AFM and paramagnetic phases occured at the Néel temperature. Although MnTiO$_3$ has a lower crystallographic symmetry than Cr$_2$O$_3$ that caused a small, non-zero SHG circular polarization dependence even in the paramagnetic phase, one may still exploit the enhanced CID in the AFM phase to record the onset of antiferromagnetism. Hence, it should also be possible to image 180° magnetic domains by measuring the difference in SHG intensity generated by reversed domains within the sample, provided the domains are large enough

to be resolved by the optical visualization system. Thus, the lower crystallographic symmetry of $MnTiO_3$ was not necessarily a hindrance to analyzing the symmetry of the antiferromagnetic phase in $MnTiO_3$.

The SHG of $MnTiO_3$ in the spin-flop phase was also measured. A magnetic field of 8 T (H_c =6.5 T), applied along the c-axis while the sample was at 1.6 K, canted the Mn^{2+} spins away from the c-axis. Fig. 3(f) shows that the transition in SHG behavior from AFM to spin-flop phase occurred at the critical magnetic field. The CID in the spin-flop phase (Fig. 3(c)) was very similar to the paramagnetic result. This was remarkable since the rotation of the spins into the ab-plane removed the trigonal axis of the zero magnetic field AFM phase, thereby lowering the magnetic symmetry group. Although the zero magnetic field AFM symmetry of $MnTiO_3$ has been reported as $\bar{3}$[14,30,31,35], it is possible that the magnetic cation sublattice still retains the twofold axes and mirror planes of the higher symmetry corundum structure (i.e. $\bar{3}$ $2/m$). Such would be the case if the anions were primarily responsible for lifting these additional symmetries. This leaves three possibilities for the magnetic point symmetry in the spin-flop phase: $\underline{2}/m$, $2/\underline{m}$, and $\bar{1}$[49]. In Cr_2O_3, the magnetic symmetry in the spin-flop phase was deduced to lie along the twofold axes ($\underline{2}/m$) in the ab-plane, rather than perpendicular to them ($2/\underline{m}$) since the CID of the SHG associated with the magnetic point group would only be zero in the case of the former symmetry[50]. In the case of $MnTiO_3$, we once again have similar selectivity using SHG analysis since only one of the possible magnetic symmetries permits zero CID contribution from the magnetic group. Since the SHG spectrum of $MnTiO_3$ in the spin-flop phase matched the paramagnetic behavior, we concluded that the CID contribution from the magnetic point symmetry was zero, which suggested that the magnetic symmetry conformed to $\underline{2}/m$, similarly as in Cr_2O_3, and which was also supported by
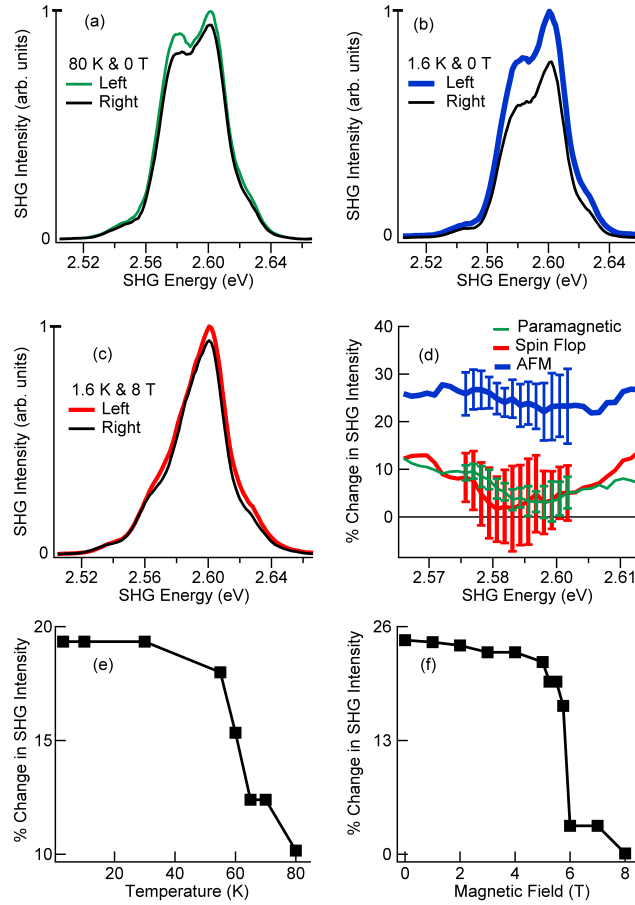

FIG. 3. (a) Circularly polarized ($\mathbf{k} \parallel c$-axis) SHG spectra in the (a) paramagnetic phase, (b) AFM phase, and (c) spin-flop phase. (d) Percent change between the left and right circular polarization SHG intensity for the three phases. At a specific point within the resonance, the difference became negligible for the paramagnetic and spin-flop phases while, in the zero-field AFM phase, the circular intensity difference remained non-zero. Error bars show the standard deviation of observations. Small variations in the absolute SHG intensities between (a), (b), and (c) could not be verified and so were removed by normalization. The variation in lineshape of (c) from (a) and (b) was caused by a small, unavoidable change in the spectrum of the exciting fundamental needed to maintain the required power output. Panels (e) & (f) show the temperature and magnetic field dependence of the percent change of circularly polarized SHG intensity, respectively.

oriented magnetization measurements (Fig. 1(e)). The $\underline{2}/m$ symmetry permits six different orientations of the spin moments within the primitive cell where the spins may cant along one of the three twofold axes of the crystal within the *ab*-plane. One possible spin domain arrangement in the spin-flop phase is depicted in Fig. 1(d). The emergence of ferrotoroidicity is not forbidden within this symmetry.

The symmetry of the spin-flop phase in $MnTiO_3$ might be further investigated by linearly polarized SHG measurements in which the incident polarization is carefully oriented in the *ab*-plane in order to further verify this evidence. However, it is advantageous to use circular polarization, since it can be implemented in multi-domain samples where the selection rules for linear polarization would be mixed. Finally, it is instructive to note that the general orientation of magnetic moments in the spin-flop phase of $MnTiO_3$ has been optically deduced via SHG analysis in spite of non-zero crystallographic SHG contributions.

V. CONCLUSION.

Second harmonic generation spectra have been successfully measured over a wide energy range in $MnTiO_3$, highlighting several SHG resonances in the visible region. These features were assigned as ZPL *d-d* magnetic-dipole transitions. The octahedral crystal field splitting energy, $10Dq$, as well as the Racah B and C parameters were calculated. A qualitative analysis of the vibronic coupling in $MnTiO_3$ was also possible by comparing the SHG and linear absorption spectra. The sharpness of the SHG lines permitted a more precise assignment of the energies for the observed optical transitions. Second harmonic spectra of $MnTiO_3$ in the paramagnetic, antiferromagnetic, and spin-flop phases were also measured for circularly-polarized excitation. Above the Néel temperature, the SHG spectra showed a circular polarization dependence, with a small dependence near the central wavelength of the resonance. The non-zero CID in the paramagnetic phase was caused by the mixing of two independent *i*-type tensor components associated with the MD transition. Below the Néel temperature, both magnetic and electric dipole transitions were allowed by symmetry; thus, there were two non-zero tensor components for both MD and ED processes. These magnetic and crystallographic components mixed to produce significant circular polarization dependence in the SHG.

In spite of the lower crystallographic symmetry of $MnTiO_3$, resulting in highly mixed SHG source terms, using SHG to map 180° antiferromagnetic domains along the *c*-axis remains feasible. SHG in the spin-flop phase further provided evidence suggestive of the magnetic moments canting towards the *a*-axis in agreement with oriented magnetization studies. SHG was an effective tool to understand the electronic structure and magnetic symmetry of $MnTiO_3$ and may also be useful in other materials with low crystallographic symmetry.

VI. ACKNOWLEDGEMENTS.

[*] Current Address: Physics Department, University of Tennessee, Knoxville, TN 37996

[†] mcgill@magnet.fsu.edu

[1] H. A. Lu, L. A. Wills, B. W. Wessels, W. P. Lin, T. G. Zhang, G. K. Wong, D. A. Neumayer, and T. J. Marks, Appl. Phys. Lett. **62**, 1314 (1993).

[2] Y. Deng, Y.L. Du, M.S. Zhang, J.H. Han, and Z. Yin, Solid State Commun. **135**, 221 (2005).

[3] S. Singh, J. P. Remeika, and J. R. Potopowicz, Appl. Phys. Lett. **20**, 135 (1972).

[4] T. Varga, A. Kumar, E. Vlahos, S. Denev, M. Park, S. Hong, T. Sanehira, Y. Wang, C. J. Fennie, S. K. Streiffer, X. Ke, P. Schiffer, V. Gopalan, and J. F. Mitchell, Phys. Rev. Lett. **103**, 047601 (2009).

[5] J. H. Haeni, P. Irvin, W. Chang, R. Uecker, P. Reiche, Y. L. Li, S. Choudhury, W. Tian, M. E. Hawley, B. Craigo, A. K. Tagantsev, X. Q. Pan, S. K. Streiffer, L. Q. Chen, S. W. Kirchoefer, J. Levy, and D. G. Schlom, Nature **430**, 758 (2004).

[6] V.V. Lemanov, A.V. Sotnikov, E.P. Smirnova, M. Weihnacht, and R. Kunze, Solid State Commun. **110**, 611 (1999).

[7] J. G. Mavroides, J. A. Kafalas, and D. F. Kolesar, Appl. Phys. Lett. **28**, 241 (1976).

[8] H. Mizoguchi, K. Ueda, M. Orita, S.-C. Moon, K. Kajihara, M. Hirano, and H. Hosono, Mater. Res. Bull. **37**, 2401 (2002).

[9] J. Z. Kong, A. D. Li, H. F. Zhai, H. Li, Q.Y. Yan, J. Ma, D. Wu, Journal of Hazardous Materials **171**, 918 (2009).

[10] G. W. Zhou and Y. S. Kang, Materials Science and Engineering: C **24**, 71 (2004).

[11] Z. Song, S. Wang, W. Yang, M. Li, H. Wang, H. Yan, Materials Science and Engineering: B **113**, 121 (2004).

[12] H. Toyosaki, M. Kawasaki, and Y. Tokura, Appl. Phys. Lett. **93**, 072507 (2008).

[13] H. Yamauchi, H. Hiroyoshi, M. Yamada, H. Watanabe, H. Takei, Journal of Magnetism and Magnetic Materials **31**, 1071 (1983).

[14] N. Mufti, G. R. Blake, M. Mostovoy, S. Riyadi, A. A. Nugroho, and T. T. M. Palstra, Phys. Rev. B **83**, 104416 (2011).

[15] B. B. V. Aken, J. P. Rivera, H. Schmid, and M. Fiebig, Nature **449**, 702 (2007).

[16] N. A. Spaldin, M. Fiebig, and M. Mostovoy, J. Phys.: Condens. Matter **20**, 434203 (2008).

[17] D. Fröhlich, St. Leute, V. V. Pavlov, R. V. Pisarev, and K. Kohn, J. Appl. Phys. **85**, 4762 (1999).

[18] D. Fröhlich, St. Leute, V. V. Pavlov, and R. V. Pisarev, Phys. Rev. Lett. **81**, 3239 (1998).

[19] M. Fiebig, V. V. Pavlov, and R. V. Pisarev, J. Opt. Soc. Am. B **22**, 96 (2005).

[20] M. Fiebig, D. Fröhlich, B. B. Krichevtsov, and R. V. Pisarev, Phys. Rev. Lett. **73**, 2127 (1994).

[21] M. Matsubara, C. Becher, A. Schmeh, J. Mannhart, D. G. Schlom, and M. Fiebig, J. Appl. Phys. **109**, 07C309 (2011).

[22] T. F. Heinz, C. K. Chen, D. Ricard, and Y. R. Shen, Phys. Rev. Lett. **48**, 478 (1982).

[23] M. Fiebig, D. Fröhlich, Th. Lottermoser, V. V. Pavlov, R. V. Pisarev, and H.-J. Weber, Phys. Rev. Lett. **87**, 137202 (2001).

[24] P. Chen, N. Lee, S. McGill, S.-W. Cheong, and J. L. Musfeldt, Phys. Rev. B 85, 174413 (2012).

[25] J. B. Goodenough and J. J. Stickler, Phys. Rev. **164**, 768 (1967).

[26] R. P. Liferovich and R. H. Mitchell, Phys. and Chem. Minerals **32**, 442 (2005).

[27] R. P. Liferovich and R. H. Mitchell, Crystallography Reports **51**, 383 (2006).

[28] G. Radtke, S. Lazar, and G. A. Botton, Phys. Rev. B **74**, 155117 (2006).

[29] A. Fukaya, A. Ito, H. A. Katori, and T. Goto, J. Phys. Soc. Jpn. **69**, 3027 (2000).

[30] W. F. Brown, S. Shtrikman, and D. Treves, J. Appl. Phys. **34**, 1233 (1963).

[31] G. Shirane, S. J. Pickart, and Y. Ishikawa, J. Phys. Soc. Jpn. **14**, 1352 (1959).

[32] D. N. Astrov, J. Exptl. Teor. Fiz. **38**, 984 (1960); Sov. Phys. JETP **11**, 708 (1960).

[33] V. J. Folen, G. T. Rado, and E. W. Stalder, Phys. Rev. Lett. **6**, 607 (1961).

[34] Yu. F. Popov, A. M. Kadomtseva, D. V. Belov, G. P. Vorob'ev, and A. K. Zvezdin, JETP Lett., **69**, 330 (1999).

[35] C. Bradley and A. Cracknell, *The Mathematical Theory of Symmetry in Solids: Representation Theory for Point Groups and Space Groups* (Oxford: Clarendon Press, 1972), p. 581.

[36] R. R. Birss, *Symmetry and Magnetism*, (North-Holland Pub. Co., Amsterdam, 1964); Rep. Prog. Phys. **26**, 307 (1963).

[37] Y. R. Shen, *The Principles of Nonlinear Optics*, (Wiley-Interscience, 1984).

[38] P. S. Pershan, Phys. Rev. **130**, 919 (1963).

[39] R. G. Burns, *Mineralogical Application of Crystal Field Theory*, (Cambridge University Press, 1993) 2nd Ed.

[40] Mark Fox, *Optical Properties of Solids*, (Oxford University Press, 2001) 1st Ed.

[41] D. D. Sell, R. L. Greene, and R. M. White, Phys. Rev. **158**, 489 (1967).

[42] J. W. Allen, R. M. Macfarlane, and R. L. White, Phys. Rev. **179**, 523 (1969).

[43] Y.-M. Chang, L. Xu, and H. W. K. Tom, Chem. Phys. **251**, 283 (2000).

[44] J. Qin, C. Yang, K. Yakushi, Y. Nakazawa, and K. Ichimura, Solid State Commun. **100**, 427 (1996).

[45] K. Okuda, K. Kurosawa, S. Saito, M. Honda, Z. Yu, and M. Date , J. Phys. Soc. Jpn. **55**, 4456 (1986).

[46] V. Grasso, F. Neri, P. Perillo, L. Silipigni, and and M Piacentini, Phys. Rev. B **44**, 11060 (1991).

[47] V. Grasso, F. Neri, L. Silipigni, and M Piacentini, Phys. Rev. B **40**, 5529 (1989).

[48] J. B. Goates, E. Lifshitz, and A. H. Francis, Inorg. Chem. **20**, 3019 (1981).

[49] M. S. Dresselhaus, G. Dresselhaus, and A. Jorio, *Group Theory: Application to the Physics of Condensed Matter*, (Springer, 2008) 1st Ed.

[50] M. Fiebig, D. Fröhlich, and H.-J. Thiele, Phys. Rev. B **54**, R12681 (1996).